Acquisition Settings for PET of ^{124}I Administered Simultaneously with Therapeutic Amounts of ^{131}I

Mark Lubberink[1], Annelies van Schie[1], Hugo W.A.M. de Jong[1], Guus A.M.S. van Dongen[2], and Gerrit J.J. Teule[1,3]

[1]Department of Nuclear Medicine and PET Research, VU University Medical Centre, Amsterdam, The Netherlands; [2]Department of Otolaryngology and Head and Neck Surgery, VU University Medical Centre, Amsterdam, The Netherlands; and [3]Department of Nuclear Medicine, Maastricht University Hospital, Maastricht, The Netherlands

Radiation dosimetry of thyroid cancer therapy with ^{131}I can be performed by coadministration of ^{124}I followed by longitudinal PET scans over several days. The photons emitted by ^{131}I may affect PET image quality. The aim of this study was to assess the influence of large amounts of ^{131}I on PET image quality and accuracy with various acquisition settings. **Methods:** Noise equivalent count (NEC) rates of ^{124}I only were measured with a standard clinical PET scanner. Apart from the standard 350- to 650-keV energy window, 425- to 650-keV and 460- to 562-keV windows were used and data were acquired both with (2-dimensional) and without (3-dimensional [3D]) septa. A phantom containing 6 hot spheres, filled with a combination of ^{131}I and ^{124}I and with a sphere-to-background ratio of 18:1, was scanned repeatedly with energy window settings as indicated and emission and transmission scan durations of 7 and 3 min, respectively. NEC rates were calculated and compared with those measured with the phantom filled with only ^{124}I. Sphere-to-background ratios in the reconstructed images were determined. One patient with known metastatic thyroid cancer was scanned using energy window settings and scan times as indicated 3 and 6 d after administration of 5.5 GBq of ^{131}I and 75 MBq of ^{124}I. **Results:** The highest ^{124}I-only NEC rates were obtained using a 425- to 650-keV energy window in 3D mode. In the presence of ^{131}I, the settings giving the highest NEC rate and contrast were 425−650 keV and 460−562 keV in 3D mode, with the clinical scans giving the highest quality images with the same settings. **Conclusion:** Acquisition in 3D mode with a 425- to 650-keV or 460- to 562-keV window leads to the highest image quality and contrast when imaging ^{124}I in the presence of large amounts of ^{131}I using a standard clinical PET scanner.

Key Words: PET; ^{124}I; dosimetry; data acquisition

J Nucl Med 2006; 47:1375–1381

There is an increasing interest in the use of the long-lived positron-emitting iodine isotope ^{124}I with PET. The most common applications of ^{124}I with PET are in thyroid disease (*1–8*) and in imaging of antibodies (*9–16*), of which the kinetics are too slow to allow the use of the common short-lived PET nuclides such as ^{18}F. Recently, the use of ^{124}I-labeled tracers for PET of apoptosis (*17,18*), insulin receptors (*19*), hypoxia (*20*), and proliferation (*21*) has been suggested. One important potential use of ^{124}I is radiation dose evaluation of thyroid cancer therapy with ^{131}I or radioimmunotherapy with ^{131}I-labeled antibodies. The distribution of ^{131}I-labeled radiopharmaceuticals can only be measured using γ-cameras without the possibility of accurate quantification. Labeling of the same substance with ^{124}I allows for the use of PET to obtain a quantitative measure of the uptake of the ^{124}I-labeled analog, which is exactly the same as the uptake of the therapeutic radiopharmaceutical. In addition to dose planning by ^{124}I PET before ^{131}I therapy (*1,11,15*), dose evaluation during therapy can be performed by coadministration of the ^{124}I-labeled radiopharmaceutical followed by serial PET scans over several days (*3,5,8*). However, the γ-radiation produced by large amounts of ^{131}I during PET measurements poses a challenge to the image quality and quantitative accuracy of PET.

^{124}I (half-life, 4.18 d) has a positron abundance of only 23% and a maximum and mean positron energy of 2,138 and 819 keV, respectively. The physical aspects of its use in PET have been characterized previously (*9,22–24*). The positron energy of ^{124}I leads to a resolution loss of about 1 mm compared with the most common PET nuclide ^{18}F (*22*). Apart from the 511-keV photons resulting from positron annihilation, the main photons emitted by ^{124}I have energies of 602, 722, and 1,691 keV, with abundances of 60%, 10%, and 11%, respectively. About half of the positron decays is followed by emission of the 602-keV photon. So-called prompt γ-coincidences involving this photon and an annihilation photon cannot be distinguished from true coincidences between 2 annihilation photons and cause a background in the PET data (*25–27*). The other emitted photons lead to an increased singles rate and, thus, to an increase in random coincidences, an effect that may be relatively larger in 2-dimensional (2D) PET than in 3-dimensional (3D) PET, with and without slice collimation, respectively, due to down scatter of higher-energy photons in the septa in 2D PET (*28*).

Received Dec. 20, 2005; revision accepted Apr. 21, 2006.
For correspondence or reprints contact: Mark Lubberink, PhD, Department of Nuclear Medicine and PET Research, VU University Medical Centre, P.O. Box 7057, 1007 MB Amsterdam, The Netherlands.
E-mail: mark.lubberink@vumc.nl

Few studies have been done to assess the PET performance of ^{124}I imaging during therapy with ^{131}I (*3,5,29*). Erdi et al. performed a dose–response study with 74−185 MBq ^{131}I in 3 patients with thyroid carcinoma (*3*). Eschmann et al. performed both clinical studies and phantom studies. They found no influence of ^{131}I activity on PET quantification, but the range of activities used in their phantom studies is not clear (*5*). Pentlow et al. performed phantom measurements in 2D mode and found increased image noise with increasing ^{131}I activity, with quantification accurate within 10% (*29*). All of these studies were done with an Advance scanner (GE Healthcare) in 2D mode using the standard energy window (300−650 keV) of the scanner.

The performance of PET of ^{124}I during therapy with ^{131}I may be influenced by the energy window settings and acquisition mode of the PET scanner. The main photons emitted by ^{131}I (half life, 8.02 d) have energies of 364, 637, and 284 keV and abundances of 82%, 7%, and 6%, respectively. The 364- and 637-keV photons fall within the standard energy window of 350−650 keV of most scanners, so these photons contribute to the singles counting rates and, consequently, the random coincidence counting rates, leading to increased image noise. Use of a narrower energy window should decrease their contribution to the randoms rate and improve image quality. Unfortunately, narrowing the energy window also decreases the sensitivity for true coincidences, which in turn reduces image quality, and an optimum setting has to be found. As mentioned earlier, published studies considering the combination of ^{124}I and ^{131}I all considered PET scans in 2D acquisition mode. However, most currently available scanners are no longer equipped with septa and are only capable of 3D imaging, so the effect of combined ^{124}I and ^{131}I administration on 3D imaging has to be investigated.

The aim of this study was to assess the influence of large amounts of ^{131}I on PET image quality and accuracy with various energy window settings and 2D and 3D acquisition modes using a standard clinical PET scanner. Phantom measurements of ^{124}I were performed both with and without the presence of ^{131}I to quantify the effect of acquisition settings on image quality, and clinical scans of a thyroid cancer patient were used to visually evaluate the optimal acquisition settings.

MATERIALS AND METHODS

PET Scanner

All measurements were made with an ECAT Exact HR+ scanner (CTI/Siemens) (*30,31*). The field of view (FOV) of this scanner is 55 cm in transaxial and 15.5 cm in axial direction. The scanner consists of 32 rings of bismuth germanate (BGO) detectors, producing 63 image planes, and is capable of imaging in both 2D (with septa) and 3D (without septa) mode. The standard energy window of the scanner is 350−650 keV. Correction for random coincidences is done online using a delayed window. Data are normalized and corrected for dead time and scatter using the methods included in the ECAT 7.2 software (CTI/Siemens) and corrected for attenuation based on a transmission scan with rotating ^{68}Ge rod sources. The standard normalization was used for all image reconstructions. The intrinsic spatial resolution of this scanner is approximately 4.5 mm, whereas the resolution obtained with the reconstruction filter used in the present study is 6.5 mm in the center of the FOV of the scanner.

Radionuclides

The iodine isotopes ^{131}I and ^{124}I were purchased from Mallinckrodt Medical BV and RITVERC Isotope Products, respectively.

^{124}I Noise Equivalent Count (NEC) Rate

A 20-cm-diameter, 20-cm-long water-filled acrylic phantom was filled with ^{124}I solution in 15 steps, with total phantom activity increasing from 0 to 87 MBq. After each addition of ^{124}I, the phantom was fixed in the center of the FOV of the scanner and six 2-min scans were made with energy windows of 350−650, 425−650, and 460−562 keV, in 2D and 3D modes.

NEC rates were calculated from the sum of all projections in each scan using a modified version of the procedure described in the NEMA 1994 standard (*32*):

$$NEC = \frac{T^2}{T + S + G + 2fD}.$$

In Equation 1, T is the trues counting rate in a 24-cm-diameter area in the center of the scanner; S and G are the scatter and prompt γ-counting rates, respectively; D is the randoms counting rate as measured in a delayed coincidence window; and f is the fraction of the sinogram occupied by the phantom, set to 0.436 to cover the central 24 cm of the sinogram. The prompt γ-counting rate G is assumed to be uniformly distributed in the sinogram (*27*). G is calculated as the mean of the 10 outermost projection bins multiplied by the number of bins within the central 24 cm of the projection. The sum of scatter and prompt γ-distributions was determined by a gaussian fit to the projection tails outside the object (*33–35*), with a constraint that the difference between the measured projection and the scatter distribution must resemble the theoretic shape of the attenuated projection of a uniform cylinder. The scatter coincidence rate S was calculated as the counting rate in the area under the central 24 cm of the gaussian fit minus the γ-coincidence rate G.

Because scatter and prompt γ-fractions are independent of the total amount of activity in the phantom, the mean of the scatter and prompt γ-fractions of the 10 scans with the highest amounts of radioactivity was calculated and subsequently applied in the NEC rate calculation of all scans.

^{124}I and ^{131}I Image Contrast and NEC Rate

The same phantom, now containing 6 hot spheres with diameters ranging from 10 to 38 mm, was filled with ^{131}I and ^{124}I. The amounts of radioactivity resembled those found in a patient a few days after high-dose therapy, starting with 75 MBq ^{131}I and 6.4 MBq ^{124}I. The sphere-to-background ratio was 18:1. The phantom was scanned 3 times during 2 wk with energy window settings as given earlier and emission and transmission scan durations of 7 and 3 min, respectively. Images were reconstructed using (Fourier rebinning and) 2D filtered backprojection applying a Hanning filter with a cutoff at 0.5 of the Nyquist frequency as implemented

in the ECAT 7.2 software. The number of counts in the sinogram tails was found to be too low to perform an accurate correction for prompt γ-coincidences using a tail fit (*27,36,37*), so this correction was omitted. Measured sphere-to-background contrasts were determined by dividing the counts per voxel measured in a region of interest placed over the center of each sphere, with size equal to the sphere size, by the counts per voxel measured in a 5-cm diameter, 15.5-cm-long volume of interest in the center of the phantom. NEC rates of this sphere phantom were calculated as described and compared with those measured with the uniform phantom filled with only ^{124}I. Scatter fractions were assumed to be identical to those determined in the NEC measurement above.

Clinical Study

One patient (76-y-old man) with known metastatic thyroid cancer was scanned after simultaneous oral administration of 5.5 GBq of ^{131}I and 75 MBq of ^{124}I. At 3 d and 6 d after administration, a whole-body scan (5 bed positions, 7-min emission, 3-min transmission) was made, followed by several static acquisitions with the same scan durations using 2D and 3D acquisition modes and the 3 different energy windows. Because of limitations in total scan duration, not all acquisition modes and energy windows could be used on each scan day. Data were corrected as described for the phantom studies. Images were reconstructed with (Fourier rebinning and) attenuation-weighted ordered-subsets expectation maximization (OSEM) (2 iterations, 16 subsets), and quality and contrast of images obtained using different energy windows were compared by a nuclear medicine physician.

RESULTS

Figure 1 shows ^{124}I NEC rates for all 3 energy window settings in both 2D and 3D modes. In 2D mode, the standard 350- to 650-keV window leads to the highest NEC rates. In 3D mode, however, the highest NEC rate is obtained with a 425- to 650-keV window. NEC rates were approximately twice as high in 3D mode, almost reaching their peak at 90 MBq. In both cases, the differences between the 350- to 650-keV and 425- to 650-keV windows are small.

Estimated scatter and prompt γ-fractions, calculated as S/(T + S) and G/(T + S + G), respectively, and the total of the 2 fractions, calculated as (S + G)/(T + S + G), are shown in Table 1 along with the estimated prompt γ-fractions in the sphere phantom containing both ^{124}I and ^{131}I. All values are expressed as the mean ± SD of 10 scans in the case of ^{124}I-only and 3 scans for the combination of ^{124}I and ^{131}I. As expected, no significant difference in prompt γ-fraction between the scans with and without ^{131}I was seen, indicating that ^{131}I does not contribute to sinogram bias and only increases image noise due to an increased random coincidence rate.

Figures 2, 3, and 4 show the results of the measurement with the sphere phantom containing both ^{124}I and ^{131}I. In 2D mode, the 425- to 650-keV window now yields the highest NEC rate and image contrast, whereas the 460- to 562-keV window gives the highest NEC rate and image contrast in 3D mode. Differences between the 2 narrow windows are small, both relating to NEC rate and image

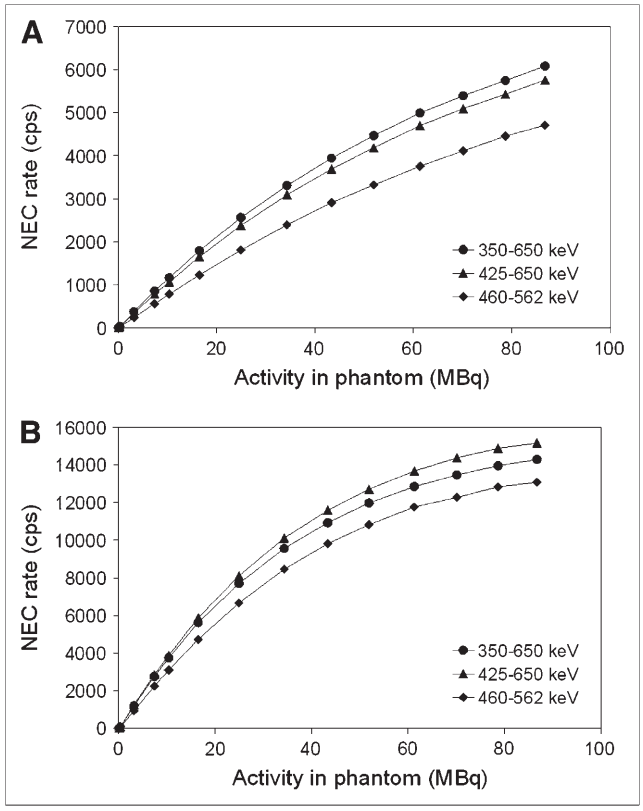

FIGURE 1. NEC rates in 2D (A) and 3D (B) modes of 20-cm-diameter, 20-cm-long phantom containing only ^{124}I.

contrast. Image contrast was better in 3D mode than in 2D mode, as shown in Figure 4.

Figure 5 shows images of the 76-y-old male patient, made at 3 or 6 d after administration of the radioactivity, as well as a fused whole-body image for orientation purposes. The 3D images appeared less noisy, with a better contrast between lesion and background, than the 2D images, with the 425- to 650-keV and 460- to 562-keV window yielding the best images. A small metastasis in the spine was only

TABLE 1
Scatter and Prompt γ-Fractions

Energy window (keV)	Scatter fraction (%)	Prompt γ-fraction (%)	Scatter + prompt γ-fraction (%)	Prompt γ-fraction + ^{131}I (%)
2D				
350−650	15.1 ± 0.7	14.3 ± 0.2	27.3 ± 1.2	14.0 ± 1.0
425−650	11.8 ± 0.8	11.8 ± 0.3	22.1 ± 1.5	12.0 ± 0.0
460−562	10.8 ± 1.0	5.7 ± 0.3	15.8 ± 1.7	5.3 ± 0.6
3D				
350−650	31.3 ± 0.5	23.7 ± 0.3	47.6 ± 1.0	26.7 ± 2.9
425−650	25.0 ± 1.1	19.1 ± 0.4	39.3 ± 2.0	20.3 ± 0.6
460−562	23.4 ± 0.8	10.0 ± 0.8	31.1 ± 2.6	11.7 ± 1.2

Data are expressed as mean ± SD.

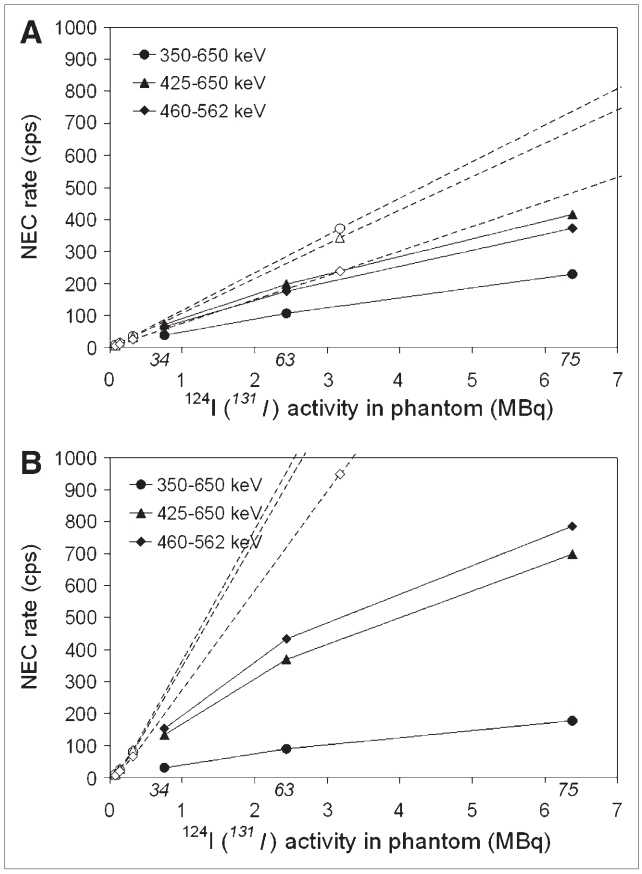

FIGURE 2. NEC rates of sphere phantom containing mixture of ^{124}I and ^{131}I, in 2D (A) and 3D (B) modes. Open symbols and dashed lines indicate NEC rates without ^{131}I.

observed using the 425- to 650-keV and 460- to 562-keV windows in 3D mode.

DISCUSSION

In the present study, the effects of γ-radiation from ^{131}I during PET scans with ^{124}I in 2D and 3D acquisition modes and applications of various energy window settings were assessed using phantom as well as patient measurements. Use of 425- to 650-keV or 460- to 562-keV energy windows in 3D mode gave the highest NEC rates and image contrasts.

The NEC rates for ^{124}I only as shown in Figure 1 can be compared with peak NEC rates of 132 and 232 kcps at approximately 215 and 110 MBq in 2D and 3D modes, respectively, for ^{11}C (*30*). 3D NEC rates are approximately a factor 15 lower for ^{124}I compared with ^{11}C. A 77% reduction in NEC rates is explained by the lower positron abundance of ^{124}I, and the further reduction is caused by the increased random rates and prompt γ-coincidences. Basically, even with the same amount of radioactivity in the patient, a 15-fold increase in scan duration is necessary to obtain the same number of NECs, and comparable image quality, in an ^{124}I scan as in a ^{18}F-FDG scan in 3D mode. On the other hand, the image contrasts in iodine scans are usually much higher than those in ^{18}F-FDG scans, which compensates for some reduction in image quality. The scatter fractions for the 350- to 650-keV window in Table 1 are slightly lower than published NEMA scatter fractions (*31*). The scatter calculation method used in the present study assumes implicitly that the scatter is zero at the outermost projection bins, which is probably not correct and causes an underestimation of the scatter fraction and an overestimation of the prompt γ-fraction. Because scatter in the outermost bins is included in the prompt γ-fraction, the sum of scatter and prompt γ-coincidences is correct, and this has no effect on the calculated NEC rates. The NEC rates are also not influenced by a slight curvature in the prompt γ-background (*27,37*), as the method used to calculate the sum of prompt γ-fraction and scatter fraction implicitly assumes a correct shape for the remaining trues projection.

NEC rates were considerably lower in the presence of ^{131}I with, at 6.4 MBq ^{124}I and 75 MBq ^{131}I, a decrease in NEC rate of 70% for the 350- to 650-keV window in 2D mode and an even larger decrease in 3D mode (Fig. 2). This decrease is caused both by a large increase in random rates, >10-fold for a 350- to 650-keV window in 3D mode, and by a decrease in net trues rates. This decrease in net trues rates, in turn, is caused by the higher dead time due to the increased singles rates. As a consequence, 2D NEC rates using the 350- to 650-keV window were actually higher than the corresponding 3D NEC rates. 3D NEC rates were still higher than 2D NEC rates for the narrower windows, where the increase in random coincidence rate is less dramatic because of the rejection of ^{131}I photons by the energy discriminator. Although it was not feasible to perform a complete NEC curve measurement with different concentration ratios of ^{131}I and ^{124}I covering the full range of radioactivity concentrations seen during therapy, the sphere phantom measurement does give some indication of the effect of the presence of ^{131}I on PET measurements with ^{124}I a few days after therapy. The results are also confirmed by the visual preference for a 425- to 650-keV or 460- to 562-keV window in the patient study. It should be noted that the results of the phantom measurement cannot be compared directly to the clinical study, as the use of OSEM with 2 iterations and 16 subsets does not lead to full convergence and, hence, not to optimal contrast recovery.

Imaging immediately after therapy would involve much larger random coincidence rates from ^{131}I, resulting in even less favorable ^{124}I imaging conditions. This will have to be confirmed in clinical studies. In addition, the effect of radioactivity outside the FOV of the scanner, as present in clinical studies, should be studied using longer phantoms or an additional phantom outside the FOV. Both of these effects would probably only strengthen the preference for a narrower energy window.

Prompt γ-correction might have improved contrasts in Figures 3 and 4, especially in the 3D scans (*27*). A bias

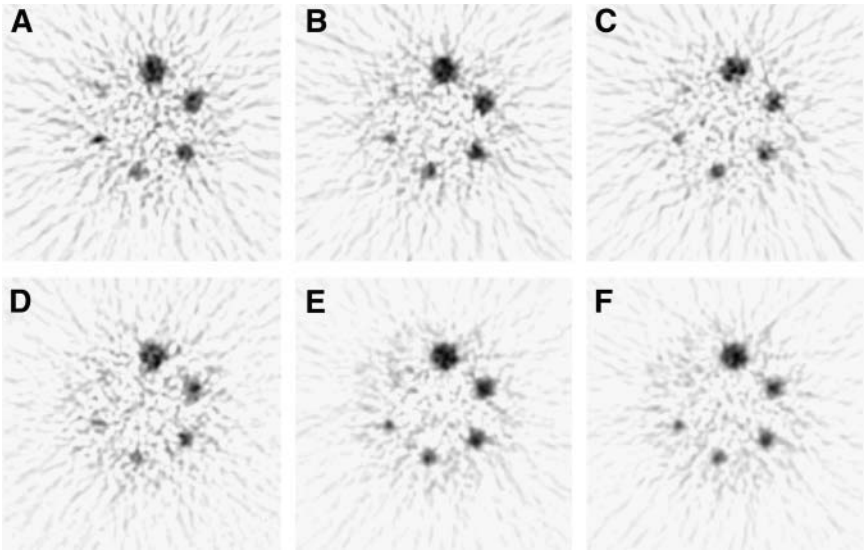

FIGURE 3. Images of sphere phantom containing 6.4 MBq ^{124}I and 75 MBq ^{131}I in 2D mode (top) and 3D mode (bottom), acquired with energy windows of 350–650 keV (A and D), 425–650 keV (B and E), and 460–562 keV (C and F).

caused by prompt γ-coincidences may explain the measured sphere-to-background ratio of 12 in the larger spheres in 3D mode, which is slightly less than expected with a recovery of approximately 80% for a 3.8-cm-diameter sphere with a similar-sized region of interest (*27*) and a true ratio of 18. The low count densities in the sinograms, however, which were even sparser for the patient study than for the phantom measurements, make accurate prompt γ-correction by tail-fit methods difficult.

Counting rate linearity, which is an important requirement for quantitative accuracy in longitudinal PET scans over a large range of amounts of radioactivity, was not investigated in this study. The dead-time correction as implemented in the ECAT 7.2 software is based on singles rates, and it was shown previously that it does not perform accurately for ^{76}Br, which also emits prompt γ-radiation (*27*). This is probably due to the relatively larger amount of detected photons outside the energy window of the scanner

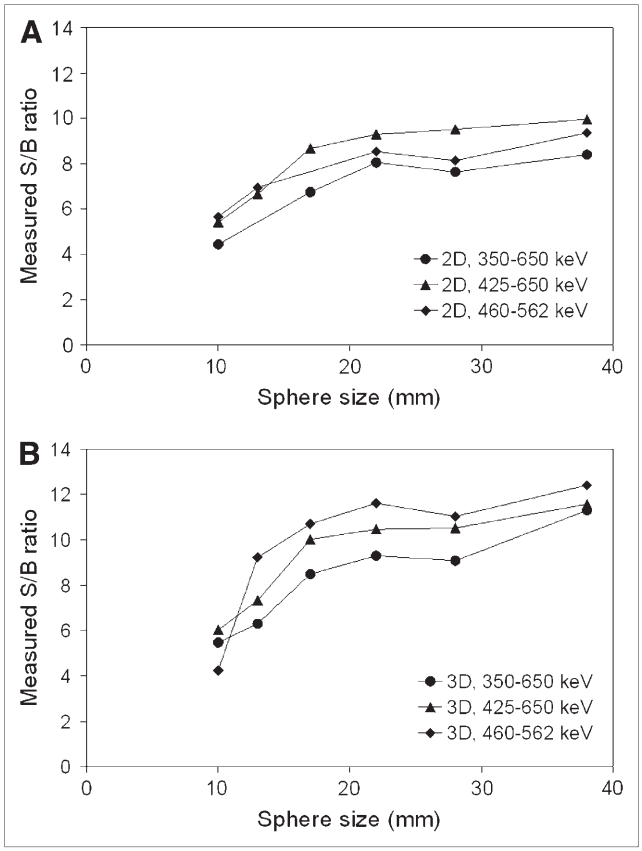

FIGURE 4. Measured sphere-to-background (S/B) ratios of images in Figure 3, at a true S/B ratio of 18 for 3 different energy window settings, in 2D mode (A) and 3D mode (B).

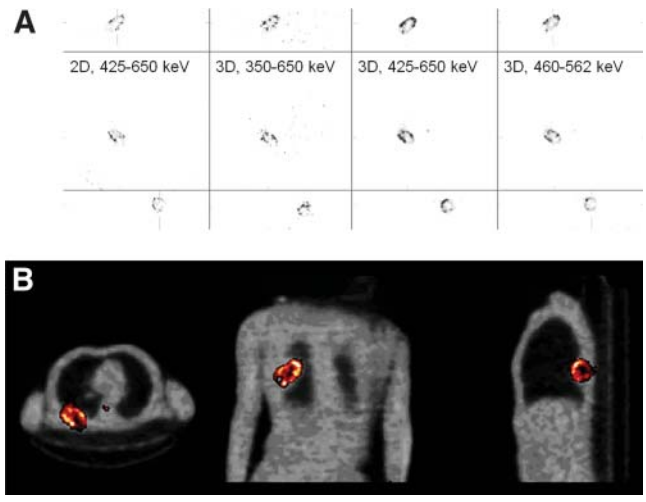

FIGURE 5. (A) Single-bed images of rib metastasis with central photopenia, acquired with 4 different acquisition settings. Top to bottom: coronal, transverse, and sagittal images. All images are at 6 d after administration, except the 350- to 650-keV image, which was taken 3 d after injection. (B) Fused emission/transmission image of 3D 425- to 650-keV whole-body scan of same patient.

for ^{76}Br than for pure positron emitters, which are rejected by the energy discriminator and not counted as singles but do contribute to dead time. For ^{124}I, however, dead-time correction of the same scanner was found to be accurate, as shown by Herzog et al. (*22*), possibly because of the much smaller numbers of single photons from ^{124}I compared with ^{76}Br. The accuracy of the standard dead-time correction for measurements of ^{124}I in the presence of large amounts of ^{131}I may be compromised because of the much larger numbers of photons coming from ^{131}I. Further studies into the counting rate linearity of ^{124}I scans in the presence of varying amounts of ^{131}I should be performed.

Many currently available scanners have faster electronics than the scanner used in the present study. In addition, these scanners use detection materials such as lutetium oxyorthosilicate (LSO), lutetium–yttrium oxyorthosilicate (LYSO), gadolinium orthosilicate (GSO), or zirconium-doped GSO (Zr-GSO), which have better energy resolution and shorter light-decay times than BGO (*38*). The better energy resolution makes it more feasible to discriminate the ^{131}I photons and ^{124}I prompt γ-rays, whereas the faster crystals and electronics lead to considerably lower random coincidences rates, which in principle makes these scanners more suitable for imaging of ^{124}I during ^{131}I therapy than BGO scanners. For these scanners, the possibility of improved ^{124}I imaging characteristics with even narrower energy windows should be evaluated. Because of the improved energy resolution of these scanners, the effect of lower trues sensitivity may be smaller than the improvement in NEC rate gained by the lower scatter and prompt γ-fractions and random coincidence rates resulting from an even narrower window. This should be validated in future studies.

The optimal energy window for PET of ^{124}I during therapy with ^{131}I—relating to both image quality and scanner performance—may be a 425- to 575-keV window in 3D acquisition mode using a clinical BGO scanner. This window is a compromise between the 425- to 650-keV and 460- to 562-keV windows found to give the best results in this study. A 425- to 575-keV window reduces the effects of the 364- and 637-keV photons from ^{131}I and the 602-keV photon from ^{124}I, without reducing trues sensitivity as much as a 460- to 562-keV window.

CONCLUSION

Dose evaluation during ^{131}I therapy can be performed by coadministration of the ^{124}I-labeled radiopharmaceutical followed by serial PET scans over several days. The γ-radiation produced by large amounts of ^{131}I during PET measurements poses a challenge to the image quality and quantitative accuracy of PET. Acquisition in 3D mode with a 425- to 650-keV or 460- to 562-keV window leads to improved image quality and contrast compared with 2D mode and to the standard energy window setting of 350−650 keV when imaging ^{124}I in the presence of large amounts of ^{131}I with the ECAT Exact HR+ scanner.

ACKNOWLEDGMENTS

The authors thank Henri N.J.M. Greuter for his assistance with the phantom measurements and Dr. Jacobus J.M. van der Hoeven for the clinical scans.

REFERENCES

1. Flower MA, al Saadi A, Harmer CL, McCready VR, Ott RJ. Dose-response study on thyrotoxic patients undergoing positron emission tomography and radioiodine therapy. *Eur J Nucl Med.* 1994;21:531–536.
2. Crawford DC, Flower MA, Pratt BE, et al. Thyroid volume measurement in thyrotoxic patients: comparison between ultrasonography and iodine-124 positron emission tomography. *Eur J Nucl Med.* 1997;24:1470–1478.
3. Erdi YE, Macapinlac H, Larson SM, et al. Radiation dose assessment for I-131 therapy of thyroid cancer using I-124 PET imaging. *Clin Positron Imaging.* 1999;2:41–46.
4. Larson SM, Robbins R. Positron emission tomography in thyroid cancer management. *Semin Roentgenol.* 2002;37:169–174.
5. Eschmann SM, Reischl G, Bilger K, et al. Evaluation of dosimetry of radioiodine therapy in benign and malignant thyroid disorders by means of iodine-124 and PET. *Eur J Nucl Med Mol Imaging.* 2002;29:760–767.
6. Freudenberg LS, Antoch G, Gorges R, et al. Combined PET/CT with iodine-124 in diagnosis of spread metastatic thyroid carcinoma: a case report. *Eur Radiol.* 2003;13(suppl 4):L19–L23.
7. Freudenberg LS, Antoch G, Jentzen W, et al. Value of ^{124}I-PET/CT in staging of patients with differentiated thyroid cancer. *Eur Radiol.* 2004;14:2092–2098.
8. Sgouros G, Kolbert KS, Sheikh A, et al. Patient-specific dosimetry for ^{131}I thyroid cancer therapy using ^{124}I PET and 3-dimensional-internal dosimetry (3D-ID) software. *J Nucl Med.* 2004;45:1366–1372.
9. Pentlow KS, Graham MC, Lambrecht RM, Cheung NK, Larson SM. Quantitative imaging of I-124 using positron emission tomography with applications to radioimmunodiagnosis and radioimmunotherapy. *Med Phys.* 1991;18:357–366.
10. Wilson CB, Snook DE, Dhokia B, et al. Quantitative measurement of monoclonal-antibody distribution and blood-flow using positron emission tomography and I-124 in patients with breast-cancer. *Int J Cancer.* 1991;47:344–347.
11. Larson SM, Pentlow KS, Volkow ND, et al. PET scanning of iodine-124-3F9 as an approach to tumor dosimetry during treatment planning for radioimmunotherapy in a child with neuroblastoma. *J Nucl Med.* 1992;33:2020–2023.
12. Daghighian F, Pentlow KS, Larson SM, et al. Development of a method to measure kinetics of radiolabelled monoclonal antibody in human tumour with applications to microdosimetry: positron emission tomography studies of iodine-124 labelled 3F8 monoclonal antibody in glioma. *Eur J Nucl Med.* 1993;20:402–409.
13. Lundqvist H, Lubberink M, Tolmachev V, et al. Positron emission tomography and radioimmunotargeting: general aspects. *Acta Oncol.* 1999;38:335–341.
14. Collingridge DR, Carroll VA, Glaser M, et al. The development of [^{124}I]iodinated-VG76e: a novel tracer for imaging vascular endothelial growth factor in vivo using positron emission tomography. *Cancer Res.* 2002;62:5912–5919.
15. Verel I, Visser GWM, Boerman OC, et al. Long-lived positron emitters zirconium-89 and iodine-124 for scouting of therapeutic radioimmunoconjugates with PET. *Cancer Biother Radiopharm.* 2003;18:655–661.
16. Robinson MK, Doss M, Shaller C, et al. Quantitative immuno-positron emission tomography imaging of HER2-positive tumor xenografts with an iodine-124 labeled anti-HER2 diabody. *Cancer Res.* 2005;65:1471–1478.
17. Keen HG, Dekker BA, Disley L, et al. Imaging apoptosis in vivo using ^{124}I-annexin V and PET. *Nucl Med Biol.* 2005;32:395–402.
18. Dekker B, Keen H, Lyons S, et al. MBP-annexin V radiolabeled directly with iodine-124 can be used to image apoptosis in vivo using PET. *Nucl Med Biol.* 2005;32:241–252.
19. Iozzo P, Osman S, Glaser M, et al. In vivo imaging of insulin receptors by PET: preclinical evaluation of iodine-125 and iodine-124 labelled human insulin. *Nucl Med Biol.* 2002;29:73–82.
20. Zanzonico P, O'Donoghue J, Chapman JD, et al. Iodine-124-labeled iodo-azomycin-galactoside imaging of tumor hypoxia in mice with serial microPET scanning. *Eur J Nucl Med Mol Imaging.* 2004;31:117–128.
21. Roelcke U, Hausmann O, Merlo A, et al. PET imaging drug distribution after intratumoral injection: the case for ^{124}I-iododeoxyuridine in malignant gliomas. *J Nucl Med.* 2002;43:1444–1451.
22. Herzog H, Tellmann L, Qaim SM, Spellerberg S, Schmid A, Coenen HH. PET quantitation and imaging of the non-pure positron-emitting iodine isotope I-124. *Appl Radiat Isot.* 2002;56:673–679.

23. Pentlow KS, Graham MC, Lambrecht RM, et al. Quantitative imaging of iodine-124 with PET. *J Nucl Med.* 1996;37:1557–1562.
24. Robinson S, Julyan PJ, Hastings DL, Zweit J. Performance of a block detector PET scanner in imaging non-pure positron emitters: modelling and experimental validation with ^{124}I. *Phys Med Biol.* 2004;49:5505–5528.
25. Martin CC, Christian BT, Satter MR, Nickerson LDH, Nickles RJ. Quantitative PET with positron emitters that emit prompt gamma rays. *IEEE Trans Med Imaging.* 1995;14:681–687.
26. Pentlow KS, Finn RD, Larson SM, Erdi YE, Beattie BJ, Humm JL. Quantitative imaging of yttrium-86 with PET: the occurrence and correction of anomalous apparent activity in high density regions. *Clin Positron Imaging.* 2000;3:85–90.
27. Lubberink M, Schneider H, Bergström M, Lundqvist H. Quantitative imaging and correction for cascade gamma radiation of ^{76}Br with 2D and 3D PET. *Phys Med Biol.* 2002;47:3519–3534.
28. Kolthammer JA, Salem N, Fiedler K, Gagnon D. Downscatter contamination from high-energy photons of ^{124}I in 2D and 3D PET. *IEEE 2004 Nuclear Science Symposium Conference Record.* 2004;6:3629–3633.
29. Pentlow KS, Mawlawi O, Daghighian F, Finn RD, Humm JL, Larson SM. Imaging of tracer amounts of I-124 in the presence of therapeutic amounts of I-131 with a standard PET scanner [abstract]. *J Nucl Med.* 1998;39(suppl):51P.
30. Adam LE, Zaers J, Ostertag H, Trojan H, Bellemann ME, Brix G. Performance evaluation of the whole-body PET scanner ECAT EXACT HR+ following the IEC standard. *IEEE Trans Nucl Sci.* 1997;44:1172–1179.
31. Brix G, Zaers J, Adam LE, et al. Performance evaluation of a whole-body PET scanner using the NEMA protocol. *J Nucl Med.* 1997;38:1614–1623.
32. *NEMA Standards Publication NU 2-1994: Performance Measurements of Positron Emission Tomographs.* Washington, D.C.: National Electrical Manufacturers Association; 1994.
33. Townsend DW, Choi Y, Sashin D, Mintun MA, Grootoonk S, Bailey DL. An investigation of practical scatter correction techniques for 3D PET [abstract]. *J Nucl Med.* 1994;35(suppl):50P.
34. Cherry SR, Huang SC. Effects of scatter on model parameter estimates in 3D PET studies of the human brain. *IEEE Trans Nucl Sci.* 1995;42:1174–1179.
35. Bendriem B, Townsend D. *The Theory and Practice of 3D PET.* Dordrecht, The Netherlands: Kluwer; 1998.
36. Beattie BJ, Finn RD, Rowland DJ, Pentlow KS. Quantitative imaging of bromine-76 and yttrium-86 with PET: a method for the removal of spurious activity introduced by cascade gamma rays. *Med Phys.* 2003;30:2410–2423.
37. Kull T, Ruckgaber J, Weller R, Reske S, Glatting G. Quantitative imaging of yttrium-86 PET with the ECAT EXACT HR+ in 2D mode. *Cancer Biother Radiopharm.* 2004;19:482–490.
38. Tarantola G, Zito F, Gerundini P. PET instrumentation and reconstruction algorithms in whole-body applications. *J Nucl Med.* 2003;44:756–769.

JNM The Journal of NUCLEAR MEDICINE

Acquisition Settings for PET of ^{124}I Administered Simultaneously with Therapeutic Amounts of ^{131}I

Mark Lubberink, Annelies van Schie, Hugo W.A.M. de Jong, Guus A.M.S. van Dongen and Gerrit J.J. Teule

J Nucl Med. 2006;47:1375-1381.

The Journal of Nuclear Medicine is published monthly.
SNMMI | Society of Nuclear Medicine and Molecular Imaging
1850 Samuel Morse Drive, Reston, VA 20190.
(Print ISSN: 0161-5505, Online ISSN: 2159-662X)

SNMMI SOCIETY OF NUCLEAR MEDICINE AND MOLECULAR IMAGING